Acta Pharmaceutica Sinica B 2024;14(4):1787−1800

Chinese Pharmaceutical Association
Institute of Materia Medica, Chinese Academy of Medical Sciences

Acta Pharmaceutica Sinica B

www.elsevier.com/locate/apsb
www.sciencedirect.com

ORIGINAL ARTICLE

Bimetallic nanoparticles as cascade sensitizing amplifiers for low-dose and robust cancer radio-immunotherapy

Yupeng Wang[a], Lina Wang[b], Tao Li[a], Min Ouyang[a], Hejian Xiong[c], Dongfang Zhou[a,*]

[a]*Department of Ultrasonic Diagnosis, Zhujiang Hospital, Key Laboratory of Mental Health of the Ministry of Education, NMPA Key Laboratory for Research and Evaluation of Drug Metabolism & Guangdong Provincial Key Laboratory of New Drug Screening, School of Pharmaceutical Sciences, Southern Medical University, Guangzhou 510515, China*
[b]*Testing and Analysis Center, Hebei Normal University, Shijiazhuang 050024, China*
[c]*Department of Mechanical Engineering, The University of Texas at Dallas, Richardson, TX 75080, USA*

Received 31 August 2023; received in revised form 10 November 2023; accepted 27 November 2023

KEY WORDS

Bimetallic nanoparticles;
Radio-immunotherapy;
Cascade sensitizing amplifier;
Oxaliplatin;
Fenton-type Haber−Weiss reaction;
Radiosensitization;
Immunogenic cell death;
Radio-resistance

Abstract Radiotherapy (RT) is one of the most feasible and routinely used therapeutic modalities for treating malignant tumors. In particular, immune responses triggered by RT, known as radio-immunotherapy, can partially inhibit the growth of distantly spreading tumors and recurrent tumors. However, the safety and efficacy of radio-immunotherapy is impeded by the radio-resistance and poor immunogenicity of tumor. Herein, we report oxaliplatin (IV)-iron bimetallic nanoparticles (OXA/Fe NPs) as cascade sensitizing amplifiers for low-dose and robust radio-immunotherapy. The OXA/Fe NPs exhibit tumor-specific accumulation and activation of OXA (II) and Fe^{2+} in response to the reductive and acidic microenvironment within tumor cells. The cascade reactions of the released metallic drugs can sensitize RT by inducing DNA damage, increasing ROS and O_2 levels, and amplifying the immunogenic cell death (ICD) effect after RT to facilitate potent immune activation. As a result, OXA/Fe NPs-based low-dose RT triggered a robust immune response and inhibited the distant and metastatic tumors effectively by a strong abscopal effect. Moreover, a long-term immunological memory effect to protect mice from tumor rechallenging is observed. Overall, the bimetallic NPs-based cascade sensitizing amplifier system offers an efficient radio-immunotherapy regimen that addresses the key challenges.

*Corresponding author.
E-mail address: dfzhou@smu.edu.cn (Dongfang Zhou).

Peer review under the responsibility of Chinese Pharmaceutical Association and Institute of Materia Medica, Chinese Academy of Medical Sciences.

https://doi.org/10.1016/j.apsb.2023.11.028

1. Introduction

Radiotherapy (RT) based on DNA damage and the generation of reactive oxygen species (ROS) has been widely utilized in clinical settings for the treatment of 65%−75% of localized solid tumors[1−3]. In recent years, immune responses triggered by RT, known as radio-immunotherapy, have attracted growing interest in suppressing tumor growth and overcoming tumor metastasis[4,5]. Cancer cells destroyed by RT can release a series of signaling molecules known as damage-associated molecular patterns (DAMPs), which work as endogenous "dangerous" signals to increase the phagocytosis of tumor antigens by DCs and activate antitumor immune response[6,7]. However, RT-induced immune responses are insufficient to meet the clinical needs[6−9]. The radioresistance and poor immunogenicity of tumors (such as inefficient maturation of dendritic cells (DCs)) are the key factors contributing to the low response of radio-immunotherapy[10−12]. High doses of RT (single dose ≧8 Gy) or the combination of RT and immune checkpoint blockade (ICB) therapy are typically employed to enhance immunogenicity at the tumor site and promote the maturation of antigen-presenting cells (APCs)[13−15]. However, these treatments often lead to inevitable toxic side effects or complications[16−18].

Platinum agents have been widely used as radio-sensitizers in clinical therapy, which potentiate DNA damage and facilitate the generation of intracellular hydrogen peroxide (H_2O_2) to enhance the efficacy of RT[19−21]. As a third-generation platinum cytotoxic drug, oxaliplatin (II) (OXA (II)) can not only sensitize RT but also elicit immunogenicity of tumor cells by inducing immunogenic cell death (ICD)[22−24]. However, a high dosage of OXA (II) is often required, and it cannot overcome the radio-resistance associated with hypoxia tumor microenvironment (TME)[25,26]. Fe-based nanoparticles (NPs) can convert H_2O_2 into highly oxidative ·OH and O_2 through a Fenton-type Haber−Weiss reaction (Supporting Information Eq. S1), thus intensifying oxidative stress and alleviating hypoxia in tumor cells[27,28]. Therefore, Fe-based NPs can serve as alternative sensitizers for radio-immun otherapy[29−31], with their efficacy dependent on the level of H_2O_2 within the TME[32,33]. Consequently, the combination of OXA (II) with Fe-based NPs is anticipated to act as a sensitizing amplifier for radio-immunotherapy through cascade reactions.

Herein, we present OXA (IV)−Fe bimetallic nanoparticles (OXA/Fe NPs) as the cascade sensitizing amplifiers for low-dose and robust tumor radio-immunotherapy (Scheme 1). OXA/Fe NPs can undergo decomposition under the reductive and acidic intracellular microenvironment to release toxic OXA (II) and free Fe^{2+}. The released OXA (II) can induce DNA damage, thus sensitizing cancer cells to RT. Simultaneously, both RT and OXA (II) contribute to an elevation in H_2O_2 level, which facilitates the Fe-initiated Fenton-type Haber−Weiss reaction, producing O_2 and highly toxic ·OH species. The O_2, a valuable source of ROS, could effectively modulate hypoxia-associated radio-resistance and amplify the sensitization effect of RT, leading to the generation of a large amount of ·OH species. The OXA (II) and the explosively produced ·OH can synergistically amplify the ICD effect after RT, promoting DC maturation and eliciting a robust and potent antitumor immune response. As expected, the OXA/Fe NPs-based low-dose radio-immunotherapy results in a significant abscopal effect on distant tumors and metastases tumors, and could establish a strong long-term immune memory effect that protects mice from re-challenged/recurrent tumors. This bimetallic NPs-based cascade sensitizing amplifier system holds great promise for future application in the next-generation radio-immunotherapy.

2. Materials and methods

2.1. Preparation and characterization of OXA/Fe NPs

Synthesis and characterization of ODex-OXA (IV)-DOP conjugate are described in detail in the Supporting Information.

ODex-OXA (IV)-DOP (100 mg) was dissolved in DMF (10 mL), and then 0.5 mL $FeCl_2·4H_2O$ solution (60 mg/mL in water) was dropped in the ODex-OXA (IV)-DOP solution with strong stirring for 30 min. Finally, the mixed solution was dialysis against ultrapure water for 24 h (dialysis bag: MWCO = 3500 Da). Then the OXA/Fe NPs solution was freeze-dried. The Pt and Fe content of OXA/Fe NPs was measured by ICP-OES. The size of the OXA/Fe NPs was measured using DLS. The morphology observed by TEM. The drug contents were measured by inductively coupled plasma optical emission spectrometry (ICP-OES).

2.2. Detection of ROS

CT26 cells were plated into 24-well plates for 24 h. Then, the cells were treated with/without free OXA (II), OXA NPs, or OXA/Fe NPs (Pt: 10 μmol/L) for 24 h and followed by exposure to X-ray irradiation (6 Gy). After incubation for another 4 h, intracellular H_2O_2 levels, ·OH levels, and overall ROS levels were measured by CLSM and flow cytometry upon addition of fluorescence probe, 10-acetyl-3,7-dihydroxyphenoxazine (ADHP for H_2O_2), Cell Meter Mitochondrial Hydroxyl Radical Detection Kit (for ·OH), or 2′,7′-dichlorofluorescin diacetate (DCFH-DA for ROS).

2.3. Cell viability assay

CT26 cells were incubated in 96-well plates with 1640 for 24 h. The medium was then replaced by free OXA (II), OXA NPs, or OXA/Fe NPs with a final Pt concentration from 0 to 40 μmol/L, and incubated for another 24 h at 37 °C. Then, CT26 cells were exposed to X-ray (0 Gy or 6 Gy) and changed to fresh 1640 medium. After further incubation of CT26 cells for 24 h, the MTT solution (20 μL, 0.5% MTT, 5 mg/mL) was added to each well, and culture for 4 h. After removing the medium, 150 μL DMSO was added to each well and shake at low speed for 2 min. Finally, the OD values of each well were measured at 490 nm with a microplate reader.

2.4. OXA/Fe NPs amplify the ICD effect of RT in vitro

For detection of CRT expression, CT26 cells were seeded into the 12-well plate (5×10^4 cells/well) and incubated for 24 h. The cells

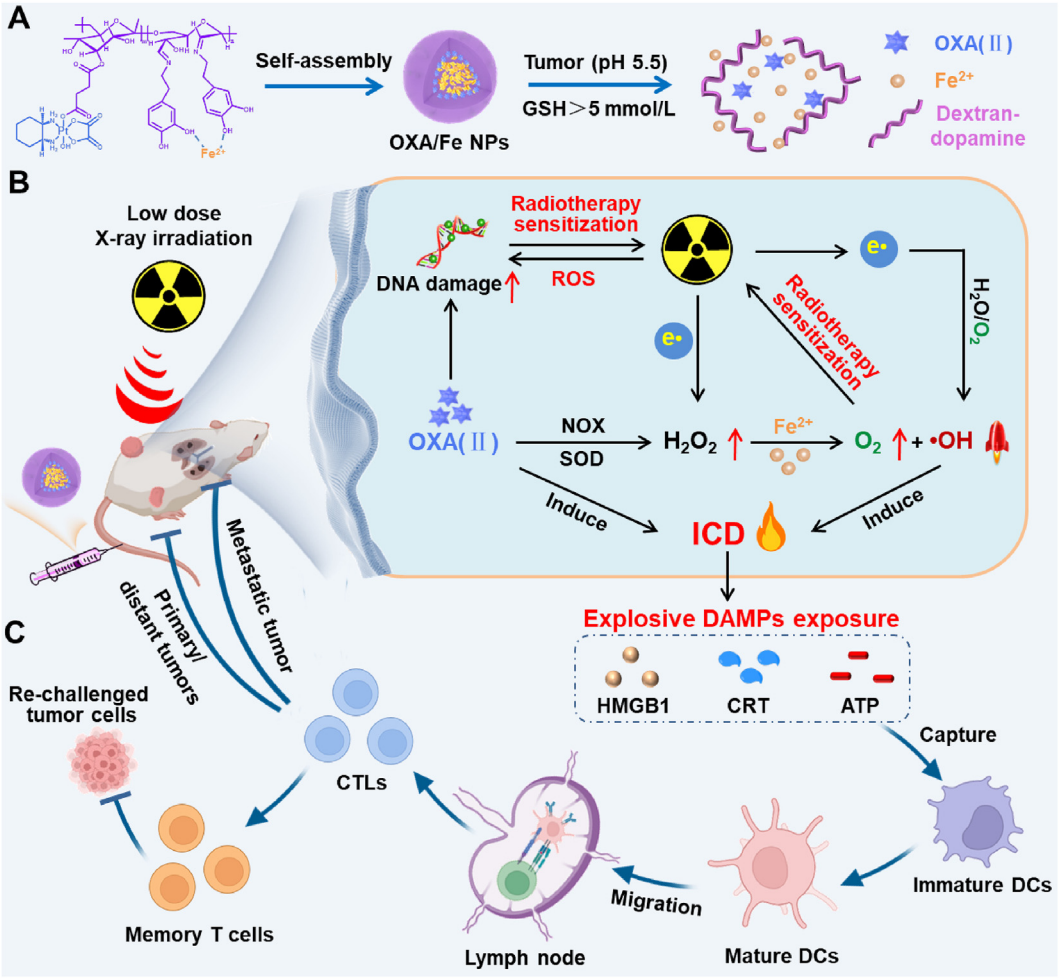

Scheme 1 Schematic illustration of the OXA (IV)−Fe bimetallic nanoparticles (OXA/Fe NPs) as cascade sensitizing amplifier for low-dose and robust cancer radio-immunotherapy. (A) Schematic design of the self-assembly and disassembly of OXA/Fe NPs; (B) After i.v. injection, OXA/Fe NPs would accumulate at the tumor site and release the active OXA (II) and Fe^{2+} in tumor cells efficiently. Upon a low-dose X-ray irradiation, the cascade reactions of the released metallic drugs can sensitize RT by inducing DNA damage, increasing ROS and O_2 levels, and then amplifying the ICD effect of RT; (C) As a result, OXA/Fe NPs-based low-dose RT could trigger a robust immune response to inhibit the distant tumors, metastatic tumors, and recurrent tumors.

were then treated with free OXA (II), OXA NPs, or OXA/Fe NPs (Pt: 10 μmol/L) for 12 h and then the cells were exposed to X-ray irradiation (0 Gy or 6 Gy). After culturing for 6 h, the CT26 cells were washed twice with PBS, fixed with 4% paraformaldehyde, and incubated with the anti-CRT antibody for 30 min, and then incubated with Alexa Fluor 488-conjugated secondary antibody for an additional 30 min. The cells were then stained with DAPI for 8 min and observed using CLSM.

For the detection of intracellular HMGB1 distribution, the cell processing procedure is the same as above. After being fixed with 4% paraformaldehyde, the cells were permeabilized with 0.1% Triton X-100 for 10 min. Afterward, the cells were blocked with 1% BSA and further incubated with anti-HMGB1 antibody for 2 h at 4 °C, and then incubated with Alexa Fluor 488-conjugated secondary antibody for 30 min. The cells were then stained with DAPI for 8 min and observed using CLSM.

Extracellular secretion of ATP was tested using an ATP assay kit. The same treatments were performed as described above. Afterward, the supernatants were collected, and the extracellular ATP content was measured with an ATP Assay Kit according to the manufacturer's instructions.

2.5. *Animal use*

Female BALB/c mice (4−5 weeks, 18 ± 2 g) and female C57 female mice (5−6 weeks, 16 ± 1 g) were bought from Guangdong Medical Laboratory Animal Center. All animal studies were executed according to the protocols of Southern Medical University approved by the Institutional Animal Care and Use Committee (IACUC). Protocols for animal experiments were approved by the NIACEC (National Institutional Animal Care & Ethical Committee) at Southern Medical University (Assurance number: NFEC-2022-071).

2.6. *In vivo tumor treatment*

To develop the subcutaneous combined bilateral tumor model, CT26 cells were injected into the left (1×10^6, primary tumor)

flank. When the primary tumors reached ~100 mm^3, the mice were used for different treatments: (G1) saline; (G2) free OXA (II); (G3) OXA/Fe NPs; (G4) X-ray irradiation; (G5) free OXA (II) + X-ray irradiation and (G6) OXA/Fe NPs + X-ray irradiation. First, free OXA (II) and OXA/Fe NPs were intravenously injected into animals at the dose of 2.5 mg/kg for Pt on Day 0. 24 h after treatment (Day 1), CT26 cells were injected into the right (2×10^5, abscopal tumor) flank, and the primary tumor on mice in the radiotherapy groups was exposed to 3 Gy X-ray radiation twice (total 6 Gy) at 0 and 12 h after injection of the CT26 cells in the abscopal site immediately. Primary and abscopal tumor sizes and body weights were monitored every 2 days.

48 h post radiotherapy (Day 3), some mice from each group were sacrificed and the maturation status of DCs in the tumor-draining lymph nodes (TDLNs) was assessed using flow cytometry. Meanwhile, to analyze treatment-induced cytokine secretion, whole blood was collected from mice. Tumor necrosis factor-α (TNF-α), interferon-γ (IFN-γ), and interleukin-12 (IL-12p40) were analyzed with ELISA kits according to the manufacturer's instructions. On Day 10 post-inoculation of the abscopal tumor (Day 11), T cell infiltration within bilateral tumors was evaluated using flow cytometry assay and immunohistochemistry (IHC).

2.7. *Statistical analysis*

All experiments *in vitro* were performed at least three times and the acquired are presented as mean ± SD. The software used for statistical analysis was GraphPad Prism 7.0. The comparison of means between the groups was performed by Student's *t*-test or analysis of ANOVA.

3. Result and discussion

3.1. *Preparation and characterization of the OXA/Fe bimetallic NPs*

Dextran with good biocompatibility is an ideal candidate for delivery systems. The oxidized dextran (ODex), featuring aldehyde and hydroxyl groups on the backbone, presents a remarkable opportunity for conjugation with diverse drugs (Scheme S1A)[34,35]. First, OXA (IV) complex (OXA (IV)-COOH) was successfully synthesized (Scheme S1B, Supporting Information Figs. S1 and S2)[36], and then conjugated onto ODex according to the previous literature (the signal of −COOH on OXA (IV) −COOH at δ 12.0 ppm disappeared in ^{1}H NMR) (Scheme S1C, Supporting Information Fig. S3). ODex-OXA (IV) conjugate was amphiphilic and could be self-assembled into nanoparticles (OXA NPs) with a spherical morphology (Size: ~85.3 nm, PDI: 0.067) (Supporting Information Fig. S4). Then, dopamine (DOP) was conjugated to the ODex-OXA (IV) conjugate *via* a reaction with the aldehyde group of ODex, forming a Schiff base in a DMF solution (the signal of O=CHR at δ 9.7 ppm disappeared in the ^{1}H NMR spectrum) (Scheme S1D, Supporting Information Fig. S5). Subsequently, $FeCl_2 \cdot 4H_2O$ was added to the above DMF solution to bind with DOP through coordination interaction by stirring at room temperature for 6 h, and then the solution was dialyzed against water to obtain ODex-OXA (IV)−Fe bimetallic nanoparticles (OXA/Fe NPs). Transmission electron microscope (TEM) image (Fig. 1A) and dynamic light scattering (DLS) (Fig. 1B) showed a uniform sphere morphology of OXA/Fe NPs with a hydrodynamic diameter around 106.6 nm (PDI: 0.083). The zeta potential of OXA NPs and OXA/Fe NPs is −7.1 and −3.6 mV, respectively (Supporting Information Fig. S6). The contents of Pt and Fe in OXA/Fe NPs were as high as 7.1% and 5.9%, respectively. The results of X-ray photoelectron spectrometry (XPS) measurement further confirmed the elemental composition in OXA/Fe NPs (Fig. 1C). The peaks at 709.5 and 723.2 eV are assigned to Fe $2p_{3/2}$ and Fe $2p_{1/2}$, respectively. The binding energy difference between the Fe $2p_{3/2}$ peak and the satellite peak for Fe $2p_{3/2}$ (715.5 eV) is approximately 6 eV, clear evidence of the existence of Fe^{2+} (Supporting Information Fig. S7A)[37]. Meanwhile, the peaks at 75.5 and 72.0 eV correspond respectively to the binding energy of Pt $4f_{5/2}$ and $4f_{7/2}$ (Fig. S7B), indicating the presence of four-valent Pt.

"On-demand" drug release within the tumor cells is important to ensure the safety and effectiveness of antitumor drugs[38]. OXA (IV) prodrug can be reduced to toxic OXA (II) by overexpressing sodium ascorbate and/or glutathione (GSH) in tumor cells[36,39]. Meanwhile, the Schiff base is widely used as an acid-labile linkage in delivery systems[35]. Therefore, OXA/Fe NPs were expected to achieve the controlled release of drugs in the intracellular reductive and acidic microenvironment of tumor cells. As shown in Fig. 1D, less than 17.6% of Pt and 12.6% of Fe were released at pH 7.4, while over 71.6% of Pt and 59.1% of Fe were released in 48 h after incubating with 5 mmol/L of GSH at pH 5.5. The XPS results revealed that the released OXA (IV) in OXA/Fe NPs (binding energies for Pt_{4f}, 78.4 and 75.2 eV) was completely reduced to OXA (II) (binding energies for Pt_{4f}, 75.5 and 72.0 eV) (Fig. 1E)[40,41]. TEM showed that OXA/Fe NPs disintegrated into small and irregular aggregates after being incubated with 5 mmol/L GSH for 48 h (Fig. 1F). No obvious changes in the morphology and size of OXA/Fe NPs were observed in PBS 7.4 (10% FBS) for 48 h (Supporting Information Fig. S8), indicating the stability of OXA/Fe NPs for long circulation.

Fenton-type Haber−Weiss reaction utilizes Fe^{2+} as the catalyst to convert H_2O_2 to O_2 and ·OH (highly oxidative free radicals)[27,28]. First, electron spin resonance (ESR) spectroscopy was used to identify the generation of ·OH. The results showed that efficient generation of ·OH, presented as the emergence of the characteristic 1:2:2:1 signals in the ESR spectrum, was only observed for the OXA/Fe NPs sample incubated with H_2O_2 (1 mmol/L), while not detected in the samples of OXA/Fe NPs alone or OXA NPs incubated with H_2O_2 (1 mmol/L) (Fig. 1J). In addition, the absorbance of methylene blue (MB, indicator of ·OH generation) significantly decreased with a time-dependent degradation manner after being co-incubated with OXA/Fe NPs and H_2O_2 (1 mmol/L), indicating the generation of ·OH (Fig. 1H, Supporting Information Fig. S9). Meanwhile, the O_2 content, measured by a portable dissolved oxygen meter, continuously increases with time in OXA/Fe NPs solution with high H_2O_2 level (1 mmol/L), indicating the remarkable O_2 generation ability of OXA/Fe NPs at high H_2O_2 level (Fig. 1I).

3.2. *Bimetallic NPs as cascade sensitizing amplifiers of low-dose RT in vitro*

The efficacy of RT critically relies on the level of ROS in the tumor during X-ray irradiation which can induce DNA damage, thus leading to cell apoptosis and necrosis[1−3]. It has been reported that OXA (II) can increase H_2O_2 levels in tumor cells by activating the nicotinamide adenine dinucleotide phosphate (NADPH) oxidases (NOXs)[42]. Meanwhile, Fe^{2+} can increase the level of

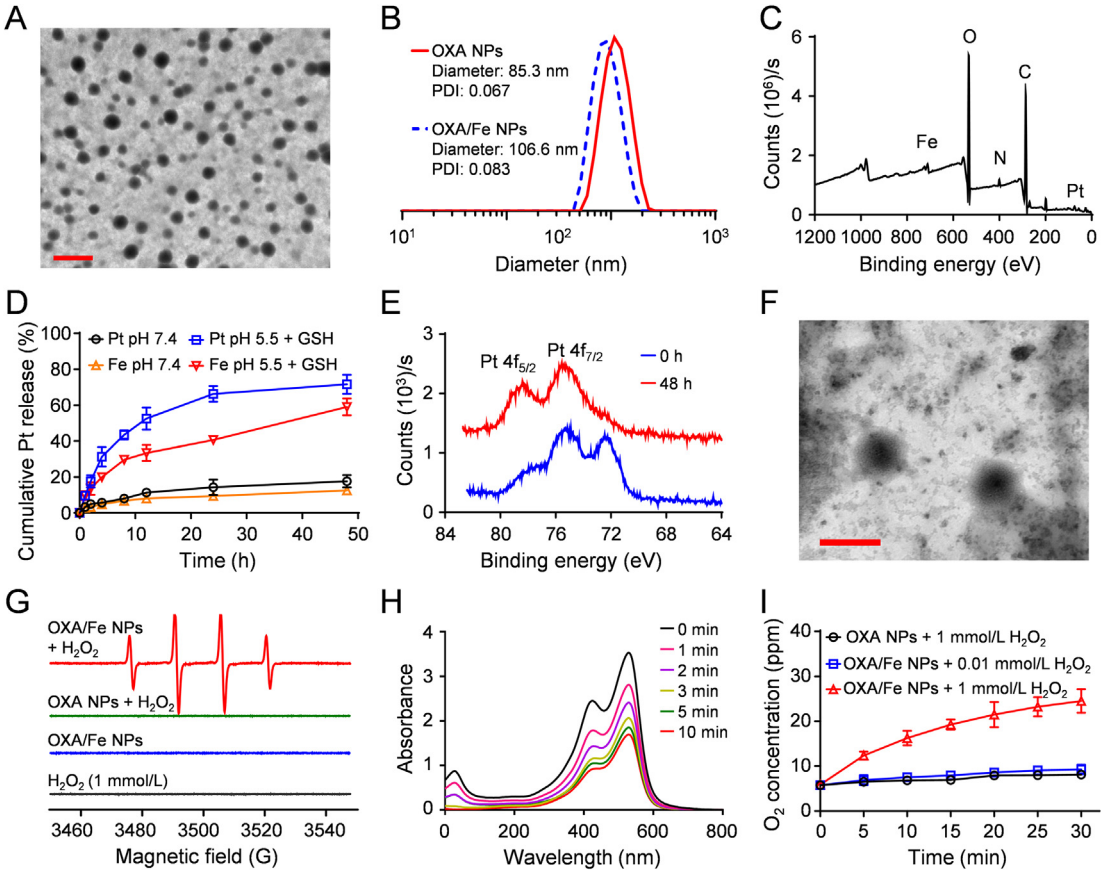

Figure 1 Preparation and characterization of the OXA/Fe bimetallic NPs. (A) TEM image of OXA/Fe NPs. Scale bar = 500 nm; (B) Size distribution of OXA NPs and OXA/Fe NPs in PBS 7.4; (C) XPS survey spectra of OXA/Fe NPs; (D) Pt and Fe release profiles of OXA/Fe NPs in PBS 7.4 without GSH and PBS 5.5 with GSH (5 mmol/L); (E) XPS curves of Pt_{4f} before and after incubation with GSH (5 mmol/L) for 48 h; (F) TEM image of OXA/Fe NPs incubation with GSH (5 mmol/L) for 48 h. Scale bar = 500 nm; (G) ESR spectra of different agents with DMPO as the radical trap; (H) Time-dependent UV−Vis spectra of MB degradation triggered by OXA/Fe NPs-mediated Fenton-type Haber−Weiss reaction in H_2O_2 solution (1 mmol/L); (I) O_2 generation curves of OXA NPs and OXA/Fe NPs in H_2O_2 solution (0.01 mmol/L or 1 mmol/L).

ROS in tumors by *in situ* catalyzing H_2O_2 to O_2 and highly oxidative ·OH[27,28]. Therefore, OXA/Fe NPs are expected as potential amplifiers for low-dose RT by enhancing ROS in tumor cells through the cascade reactions (Fig. 2A). First, the cellular internalization of OXA/Fe NPs is mediated by endocytosis (Supporting Information Fig. S10)[43], as evidenced by a time-dependent increase in drug uptake on CT26 cells. Notably, OXA/Fe NPs (81.6 ± 9.4 ng Pt/10^6 cells) exhibited a 1.46-fold higher uptake than free OXA (II) (55.7 ± 6.3 ng Pt/10^6 cells) in CT26 cells at 12 h (Supporting Information Fig. S11). Then, the levels of H_2O_2 in CT26 cells, after incubation with different treatments, were explored using 10-Acetyl-3,7-dihydroxyphenoxazine (ADHP) as the fluorescent probe and Hydrogen Peroxide Assay Kit ab102500 as a quantitative test. As expected, the combined treatment of X-ray irradiation (6 Gy) and monometallic platinum drugs (OXA (II), OXA NPs) can significantly increase the intracellular H_2O_2 levels (Fig. 2B), about 2.8 folds of the control group and 1.9 folds of the X-ray irradiation group (Fig. 2C and D). The intracellular H_2O_2 levels decreased slightly in the bimetallic OXA/Fe NPs group with/without X-ray irradiation, which may be caused by the decomposition of H_2O_2 catalyzed by released iron ions. Subsequently, the production of ·OH in cells was measured by the ·OH detection kit (Red fluorescence). As shown in Fig. 2B, the intracellular red fluorescence was significantly enhanced after being treated with OXA/Fe NPs, proving the production of ·OH through a Fenton-type Haber−Weiss reaction. Meanwhile, the combined treatment of X-ray irradiation and platinum drugs (OXA (II), OXA NPs, and OXA/Fe NPs) could also increase the red fluorescence of ·OH in CT26 cells compared with the X-ray irradiation treatment alone, especially the most obviously enhanced red fluorescence could be observed after being treated with bimetallic OXA/Fe NPs plus X-ray irradiation. Flow cytometry analysis showed that the mean fluorescence intensity of ·OH in CT26 cells treated with OXA/Fe NPs plus X-ray radiotherapy was about 8.3- and 3.4-fold higher than that detected in cells treated with the X-ray radiotherapy alone and OXA/Fe NPs alone, respectively (Fig. 2D). Furthermore, the intracellular holistic ROS level after treatment with OXA/Fe NPs plus X-ray irradiation, which was detected by the 2,7-dichlorofluorescein diacetate (DCFH-DA) fluorescent probe, was about 7.7 and 1.9 times of the X-ray irradiation group or the OXA (II) plus X-ray irradiation groups (Fig. 2D). Thus, OXA/Fe NPs can act as the ROS amplifier (especially ·OH amplifier) in tumor cells through the cascade reactions under X-ray irradiation.

Hypoxia TME is an important cause of radio-resistance and immune tolerance, which fails radio-immunotherapy[44]. To further investigate whether OXA/Fe NPs could alleviate hypoxia, Image-iT® Hypoxia Reagent was used as a probe to detect the hypoxia

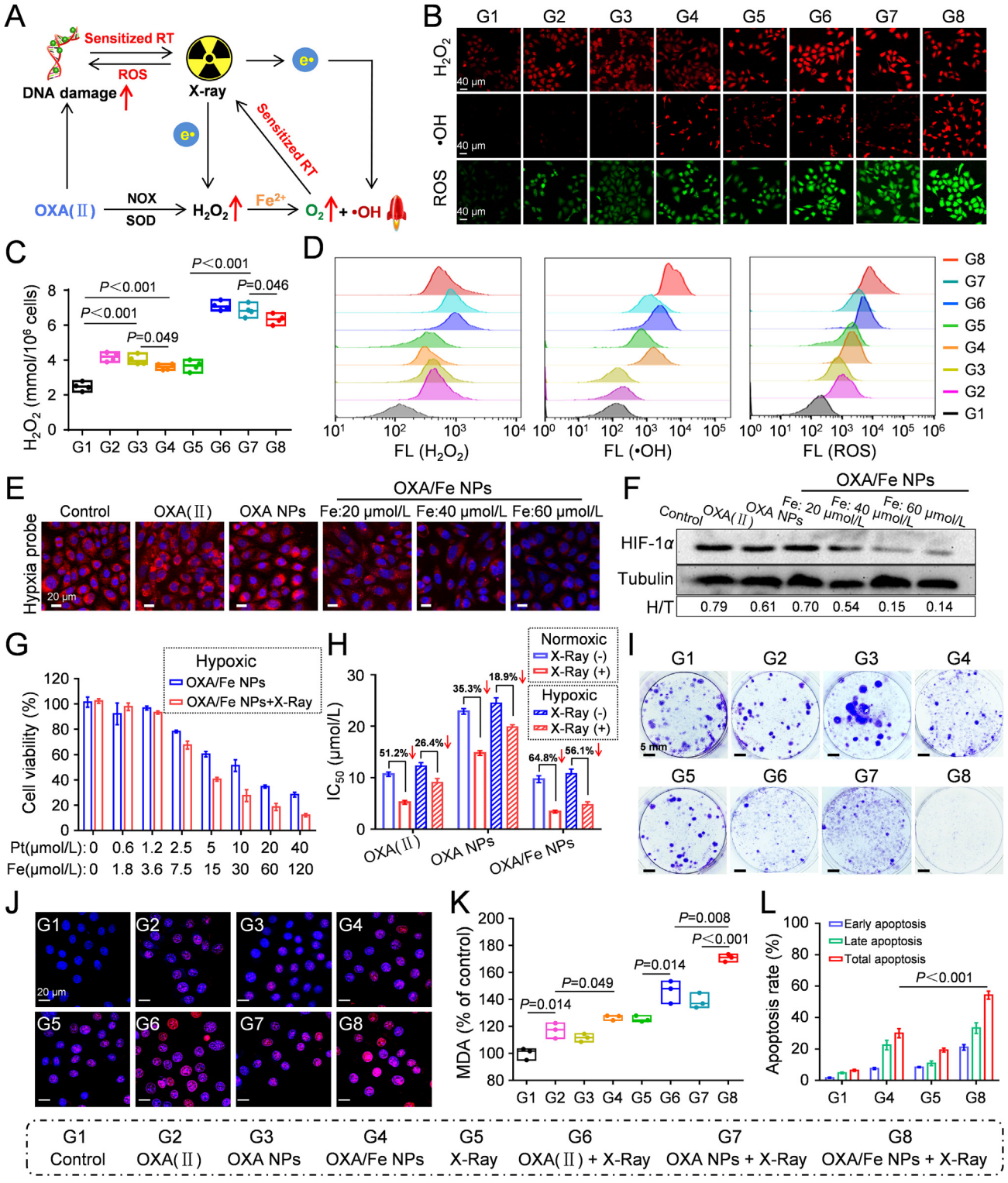

Figure 2 Bimetallic NPs as a cascade sensitizing amplifier of low-dose RT *in vitro*. (A) Illustration of OXA/Fe NPs for sensitizing cancer RT by cascade reaction; (B) Intracellular H_2O_2 level, ·OH generation, and ROS generation detected by fluorescent probe. Scale bar = 40 μm; (C) Quantitative analysis of intracellular H_2O_2 levels by H_2O_2 Assay Kit. Data are presented as mean ± SD (n = 4); (D) Quantitative analysis of intracellular H_2O_2, ·OH and ROS levels by flow cytometry; (E) Hypoxia fluorescence images of CT26 cells by staining with Image-iT® Hypoxia Reagent (Red); (F) Western blot assays of HIF-1α expressions in CT26 cells; (G) Synergistic therapeutic effects of CT26 cells treated with OXA/Fe NPs with/without X-ray irradiation (6 Gy) under hypoxic conditions. (H) IC_{50} values of OXA (II), OXA NPs, and OXA/Fe NPs on CT26 cells with/without X-ray irradiation under normoxic or hypoxic conditions; (I) Representative images of colony formation assay of CT26 cells; (J) DNA double-strand breaks in CT26 cells after different treatments. The nuclei were stained by DAPI (blue) and γ-H2AX (red). Scale bar = 20 μm; (K) Lipid peroxidation levels of CT26 cells evaluated by a Malondialdehyde assay kit; (L) Percentage of apoptotic CT26 cells after different treatments. Data are presented as mean ± SD (n = 3).

level of cancer cells. Strongly expressed red fluorescence could be observed in the cells under low oxygen condition (1% O_2). However, the fluorescence intensity decreases proportionally after being treated with different concentrations of OXA/Fe NPs, demonstrating that the hypoxia could be relieved by OXA/Fe NPs (Fig. 2E, Supporting Information Fig. S12). Moreover, the western blotting assay showed a significant reduction in the expression of hypoxia-induced factor 1α (HIF-1α) protein in CT26 cells following treatment with OXA/Fe NPs, while OXA (II) and OXA NPs groups had no significant effect on the expression of HIF-1α protein (Fig. 2F). This result further indicated that OXA/Fe NPs can catalyze H_2O_2 to produce O_2 and alleviate hypoxia of cancer cells. The O_2 served as a valuable source of ROS to modulate hypoxia-induced radio-resistance, further amplifying the generation of ·OH.

Encouraged by the above results, the amplified sensitization effect of OXA/Fe NPs on low-dose X-ray-elicited cytotoxicity in CT26 cells was further explored. The MTT results showed that both the monometallic platinum drugs (OXA (II), OXA NPs) and bimetallic OXA/Fe NPs can decrease the cell viability in CT26 cells in a concentration-dependent manner (Fig. 2G, Supporting Information Figs. S13 and S14). Indeed, upon single low-dose X-ray irradiation (6 Gy), OXA/Fe NPs had a better sensitization effect on cytotoxicity than monometallic platinum drugs under normoxic or hypoxic conditions, while only X-ray exposure (2, 4 and 6 Gy) did not exhibit any cytotoxicity towards cancer cells (Supporting Information Fig. S15). The sensitization effects of monometallic platinum drugs (OXA (II), OXA NPs) on X-ray irradiation showed weakened in hypoxic condition compared to normoxic condition, while OXA/Fe NPs maintained an excellent sensitization effect on X-ray irradiation even under hypoxic condition. For instance, the IC_{50} values of Pt in the OXA/Fe NPs plus irradiation group diminished by 64.8% (Pt: 3.41 μmol/L) and 56.1% (Pt: 4.72 μmol/L) in comparison to those of OXA/Fe NPs alone under normoxic condition (Pt: 9.71 μmol/L) and hypoxic condition (Pt: 10.75 μmol/L), respectively (Fig. 2H). These MTT results are in good agreement with the above results of ROS expression and O_2 generation, indicating that the OXA/Fe NPs could boost the anticancer effect of X-ray irradiation as a sensitizing amplifier. The lowest percentage of colonies can be found in the OXA/Fe NPs plus X-ray irradiation (6 Gy) group, further giving evidence that the OXA/Fe NPs possess an amplified sensitization effect on RT (Fig. 2I). On the other hand, the reductive level in normal cells is lower than that in cancer cells, leading to the slow release of OXA (II) from OXA/Fe NPs in normal cells. Therefore, the cytotoxicity of OXA/Fe NPs to normal cells, such as LO2 (Supporting Information Fig. S16) and Raw267.4 (Supporting Information Fig. S17), is reduced compared with OXA (II).

Then, the anticancer biological effects of OXA/Fe NPs-amplified RT were verified. DNA damage is the most lethal lesion induced by platinum anticancer drugs and X-ray irradiation. Therefore, γ-H2AX assay was used to measure the content of DNA lesions in CT26 cells. As shown in Fig. 2J, obviously fluorescence of γ-H2AX can be observed from the OXA/Fe NPs plus X-ray irradiation group, which was stronger than that of X-ray irradiation alone treatment group or monometallic platinum drugs plus X-ray irradiation treatment groups, suggesting that the OXA/Fe NPs amplified RT could lead enhanced DNA damage. High ROS concentration in cancer cells, especially ·OH, could also cause lipid peroxidation, and oxidation of amino acids in proteins, which may render cellular dysfunction[45]. Therefore, a higher level of lipid peroxidation can be observed from the OXA/Fe NPs plus X-ray irradiation group (~170.8% of control) in comparison with other groups (Fig. 2K). Finally, Annexin V/PI apoptosis staining assay showed that cells treated with OXA/Fe NPs plus X-ray irradiation (6 Gy) owned a remarkably higher percentage of the apoptotic cells (54.3%) than that of X-ray irradiation treatment alone (19.3%) or OXA/Fe NPs treatment alone (30.1%) (Fig. 2L, Supporting Information Fig. S18). Taken together, OXA/Fe NPs possess an amplified sensitization effect for low-dose RT through increased intracellular ROS level and relieved hypoxia level of cancer cells.

3.3. *Bimetallic NPs amplify the ICD effect after low-dose RT for immune activation in vitro*

The primary limitation of radio-immunotherapy lies in its inability to induce sufficient ICD effect, which is crucial for triggering effective immune responses[8,46]. Previous studies have reported that both OXA (II) and Fe-based Fenton-type Haber–Weiss reaction can elicit the ICD effect to stimulate antitumor immune responses[24,31]. Given the aforementioned observations, we were intrigued to see if the OXA/Fe NPs could synergistically enhance the ICD effect and amplify subsequent antitumor immunity when combined with low-dose RT. CLSM analysis (Fig. 3A) demonstrated that OXA/Fe NPs plus X-ray irradiation treatment resulted in a significantly high expression (green) of calreticulin (CRT, eliciting phagocytosis of the dying tumor cells by the dendritic cells (DCs)) on the surface of CT26 cells, while OXA/Fe NPs treatment and low-dose X-ray irradiation (6 Gy) treatment resulted in a moderate induction of CRT expression. High mobility group box 1 (HMGB1) is released from the nucleus during cell death, which could promote DC maturation and antigen presentation to cytotoxic T lymphocytes (CTLs)[6,7]. CLSM analysis revealed that HMGB1 (green) was primarily located in the nucleus of cells in the control group, whereas cells treated with OXA/Fe NPs plus X-ray irradiation exhibited a marked reduction of nuclear HMGB1, suggesting an enhanced translocation of HMGB1 (Fig. 3B). Furthermore, after treating with OXA/Fe NPs plus X-ray irradiation, the level of ATP in the supernatants of CT26 cells was 2.89- and 1.34-fold higher than those treated with single X-ray irradiation or OXA (II) plus X-ray irradiation, respectively (Supporting Information Fig. S19).

ICD of cancer cells leads to the release of “find-me” signals that promote phagocytosis of dying tumor cells by DCs, which can elicit DC maturation and activate the adaptive immune response[47,48]. In this study, CT26 cells were treated with various interventions and then co-cultured with bone marrow dendritic cells (BMDCs) to examine the maturation of BMDCs (Fig. 3C). The results demonstrated that the proportion of mature BMDCs ($CD80^+CD86^+$) reached approximately 59.76% in the OXA/Fe NPs plus X-ray treatment group (Supporting Information Fig. S20), which was 2.1- and 1.2-fold higher compared to the X-ray irradiation treatment group or OXA (II) plus X-ray irradiation treatment group, respectively (Fig. 3D). Enzyme-linked immune sorbent assay (ELISA) also showed that CT26 cells pretreated with OXA/Fe NPs plus X-ray irradiation can trigger higher levels of secretion of IL-12p40, TNF-α, and IFN-γ (Fig. 3E and F) by DCs compared to the other groups. All these results

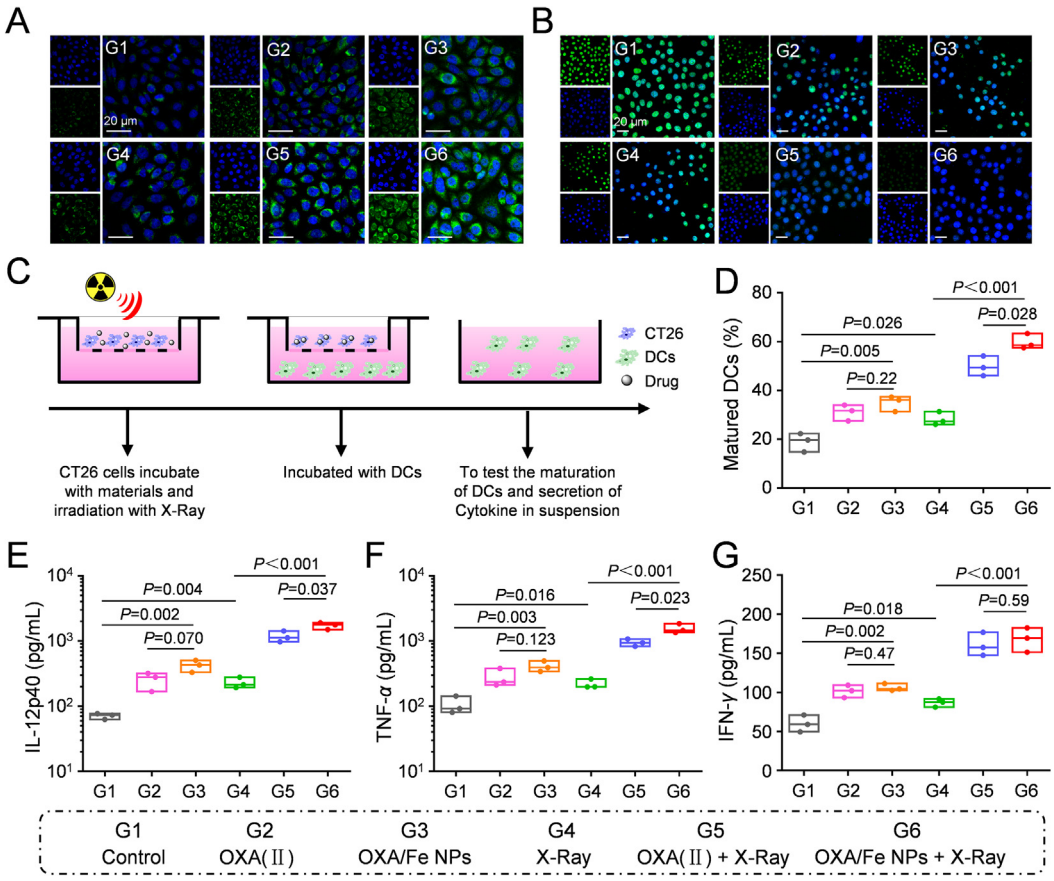

Figure 3 Bimetallic NPs amplify the ICD effect after low-dose RT for immune activation *in vitro*. CLSM images of (A) CRT exposure on the surface of CT26 cells, scale bar = 20 μm, and (B) HMGB1 release from CT26 cells after incubation with 1640 medium, OXA (II), or OXA/Fe NPs with/without X-ray irradiation (6 Gy). Scale bar = 20 μm; (C) Scheme showing the design of the transwell system experiment. CT26 tumor cells were placed in the upper chamber, and DCs were cultured in the lower chamber; (D) Flow cytometry statistic data for *in vitro* DC maturation ($CD86^+CD80^+$) after various treatments; Secretion of (E) IL-12p40, (F) TNF-α, and (G) INF-γ in DC suspensions measured by ELISA. Data are presented as mean values ± SD (n = 3).

revealed that OXA/Fe NPs plus X-ray irradiation can amplify the ICD effect of cancer cells to promote DC maturation for enhanced tumor radio-immunotherapy.

3.4. *Biodistribution of bimetallic NPs in vivo*

The biodistribution of OXA/Fe NPs in BALB/c mice with CT26 tumor was investigated. First, fluorescence imaging of the mice revealed an increase of IR780 fluorescence signal in the tumor after intravenous injection of OXA/Fe NPs loaded IR780 (IR780@OXA/Fe NPs), reaching a plateau at 24 h post-injection (Supporting Information Fig. S21). Additionally, the pharmacokinetics and biodistribution of OXA/Fe NPs were assessed using ICP-MS measurement. OXA/Fe NPs exhibited a significantly prolonged blood circulation time (half-life, $t_{1/2}$ = 7.36 h) compared to free OXA (II) ($t_{1/2}$ = 1.21 h) (Fig. S21). The intratumoral distribution of Pt from OXA/Fe NPs was higher than that of free OXA (II) at different time points after injection, which could be attributed to the prolonged blood circulation time of OXA/Fe NPs (Supporting Information Fig. S22). Meanwhile, the ICP analysis and Prussian blue staining also revealed an increase in iron content within the tumors following the administration of OXA/Fe NPs, further confirming the successful delivery of iron ions to the tumor site (Fig. S22).

3.5. *In vivo therapeutic efficacy of bimetallic NPs-amplified radio-immunotherapy on subcutaneous combined bilateral tumor model*

Subsequently, we embarked on investigating whether the potent immune responses induced by OXA/Fe NPs-based low-dose RT could effectively suppress the growth of tumor cells on a subcutaneous combined bilateral CT26 tumor model. In this model, 1×10^6 CT26 colorectal cancer cells were implanted on the left flank regions of BALB/c mice, representing the primary tumors that received direct RT. Once the primary tumors reached a volume of approximately 100 mm^3, the mice were randomly divided into six groups: (G1) Saline; (G2) free OXA (II); (G3) OXA/Fe NPs; (G4) X-ray irradiation; (G5) free OXA (II) plus X-ray irradiation; and (G6) OXA/Fe NPs plus X-ray irradiation. Intravenous injection of free OXA (II) and OXA/Fe NPs was administered at a low dose of 2.5 mg/kg for Pt. Twenty-four hours after administration, 2×10^5 CT26 cells were implanted on the right flank regions of BALB/c mice, representing abscopal tumors without

direct chemotherapy and RT. Subsequently, the primary tumors were irradiated with X-ray at a low dose of 3 Gy twice (total 6 Gy). Both the sizes of primary and abscopal tumors were monitored (Fig. 4A).

The results showed a limited tumor inhibitory effect of X-ray irradiation alone, free OXA (II), or OXA/Fe NPs for the primary tumors and the abscopal tumors (Fig. 4B, Supporting Information Figs. S23 and S24). OXA (II) plus X-ray irradiation treatment showed a moderate tumor growth inhibition efficacy for both primary and abscopal tumors, while the tumors are almost completely inhibited after being treated with OXA/Fe NPs plus X-ray irradiation. The Hematoxylin−eosin (H&E) (Supporting Information Fig. S25) and terminal deoxynucleotidyl transferase-mediated dUTP nick-end labeling (TUNEL) staining (Supporting Information Fig. S26) of the primary and abscopal tumor tissues further showed that OXA/Fe NPs-based radio-immunotherapy markedly increased necrosis and apoptosis rates compared to the other treatments. More importantly, OXA/Fe NPs plus X-ray irradiation had excellent biosafety in mice. Compared with the saline treatment group, there was no evident change in the mice weight treated with OXA/Fe NPs + X-ray irradiation till the end of the study (Fig. 4D). Serum biochemical markers (aminotransferase (AST) and alanine aminotransferase (ALT), creatinine (CREA), and blood urea nitrogen (BUN)) of mice received OXA/Fe NPs + X-ray irradiation were within the normal ranges (Supporting Information Table S1). Furthermore, no pathological damages were observed in the H&E-stained images of tissues in the OXA/Fe NPs + X-ray irradiation group (Supporting Information Fig. S27). Taken together, the aforementioned findings collectively demonstrated that OXA/Fe NPs exhibited amplified radio-immunotherapy on both the primary and the abscopal tumors while ensuring biosafety.

To understand the potential antitumor immune mechanisms by the OXA/Fe NPs-amplified radio-immunotherapy, the tumor-draining lymph nodes (TDLNs) and tumor tissues of mice in different treatment groups were harvested for systematic analysis. First, the immunofluorescent and immunohistochemical examination showed that the signals of hypoxia-probe (Image-iT® Hypoxia Reagent) and expression of HIF-1α (Fig. 4E, Supporting Information Fig. S28) have an obvious decrease in tumors 24 h after intravenous injection with OXA/Fe NPs (Day 1), indicating that OXA/Fe NPs can effectively alleviate the hypoxic of the tumor. Two-day post-X-ray irradiation (Day 3), mice were sacrificed to assess the *in vivo* activation of antitumor immunity. The immunofluorescent and flow cytometry assay showed that OXA/Fe NPs combined with low-dose RT significantly amplified the ICD effect by promoting CRT exposure (Fig. 4F, Supporting Information Fig. S29) and HMGB1 release (Supporting Information Fig. S30) of tumor cells *in vivo*. The enhanced DAMP exposure in tumors can facilitate the maturation of antigen-presenting cells (APCs). Therefore, DC maturation in the TDLNs was also detected with flow cytometric examination on Day 3 (Supporting Information Fig. S31). The X-ray irradiation treatment and OXA/Fe NPs treatment moderately facilitated the DC maturation from 13.3 ± 3.2% to 22.9 ± 2.1% and 25.4 ± 3.5%, respectively, compared to that of the saline group. As expected, OXA/Fe NPs plus X-ray irradiation treatment further increased the ratio of maturation DCs to 47.5 ± 5.7%, which was 2.16 and 1.32 times of irradiation alone or OXA (II) plus X-ray irradiation, respectively (Fig. 5G, Supporting Information Fig. S32).

The mature DCs play a crucial role in antigen presentation to T lymphocytes, thus promoting intratumoral infiltration of CTLs[47−49]. It is well-known that $CD8^+$ T cells could kill cancer cells by releasing the cytotoxins−IFN-γ, perforin, and granzymes[50]. On the other hand, $CD4^+$ T cells could induce inflammatory cell death of immuno-escaped tumor cells[51,52]. Therefore, the infiltration of $CD4^+$ T cells and $CD8^+$ T cells in the primary and abscopal tumors were examined by flow cytometric on Day 10 post irradiation treatment (Day 11). The percentage of $CD4^+$ T cells and $CD8^+$ T cells in the primary tumors (Supporting Information Fig. S33) of the OXA/Fe NPs plus X-ray irradiation group showed an obvious increase compared to those with OXA/Fe NPs alone, X-ray irradiation alone, or OXA (II) plus X-ray irradiation groups. In particular, the percentage of $CD4^+$ T cells (Supporting Information Fig. S34) and $CD8^+$ T cells (Fig. 4H, Fig. S34) in the abscopal tumor of the OXA/Fe NPs plus X-ray irradiation group increased, which was 2.09 and 2.36 folds of that in the X-ray irradiation group, or 1.18 and 1.36 folds of that in the OXA (II) plus X-ray irradiation group. Furthermore, OXA/Fe NPs plus X-ray irradiation was most efficient in inducing the intratumoral infiltration of interferon γ-positive (IFN-γ^+) cytotoxic T lymphocytes ($\approx$42.5 ± 2.6% in the primary tumor, and $\approx$39.7 ± 3.1% in the abscopal tumor), which was 1.52- and 1.19-fold higher than that of X-ray irradiation group and OXA (II) plus X-ray irradiation group, respectively (Fig. 4I, Supporting Information Fig. S35). The immunohistochemical staining also revealed that OXA/Fe NPs plus X-ray irradiation increased the intratumoral infiltration density of $CD8^+$ T cells compared to other groups (Supporting Information Fig. S36). The secretion levels of TNF-α, IFN-γ, and IL-12p40 (stimulating factor that promotes differentiation and proliferation of T lymphocytes and NK cells)[53] for mice treated by OXA/Fe NPs plus X-ray irradiation appeared to be much higher than that in other treatment groups (Fig. 4J, Supporting Information Fig. S37). Taken together, all the above results indicated that OXA/Fe NPs-based low-dose RT can facilitate DCs maturation and remodel the tumor immune microenvironment, resulting in an excellent inhibition effect on the growth of primary tumors and secondary tumors.

3.6. *In vivo therapeutic efficacy of bimetallic NPs-amplified radio-immunotherapy on lung metastasis model*

To further evaluate the efficacy of amplified radio-immunotherapy of OXA/Fe NPs *in vivo*, a lung metastasis model was conducted on C57 female mice (Fig. 5A). In this model, 2×10^6 luciferase B16 (B16-luc) cells were intravenously injected into the mice. After 7 days, the presence of B16-luc tumors can be detected in the lung of mice by intraperitoneal injection of D-luciferin (Supporting Information Fig. S38). All the mice were then randomly divided into six groups, and *in vivo* bioluminescence imaging was carried out after various treatments (Fig. 5B). It was found that the tumor metastases were inhibited effectively for mice treated with OXA/Fe NPs + X-ray irradiation, in marked contrast to the other treatment groups, in which large-area visible metastasis was noted. Moreover, no single death of mice treated with OXA/Fe NPs + X-ray irradiation was observed until Day 15 (Fig. 5C). The metastatic nodules in the lungs were counted at the end of treatment. As shown in Fig. 5D, the lowest number of metastasis nodes was observed in the lungs of the OXA/Fe NPs + X-ray irradiation group among all six groups. These results demonstrated that the OXA/Fe NPs-amplified radio-immunotherapy could suppress the metastasis of tumors efficiently.

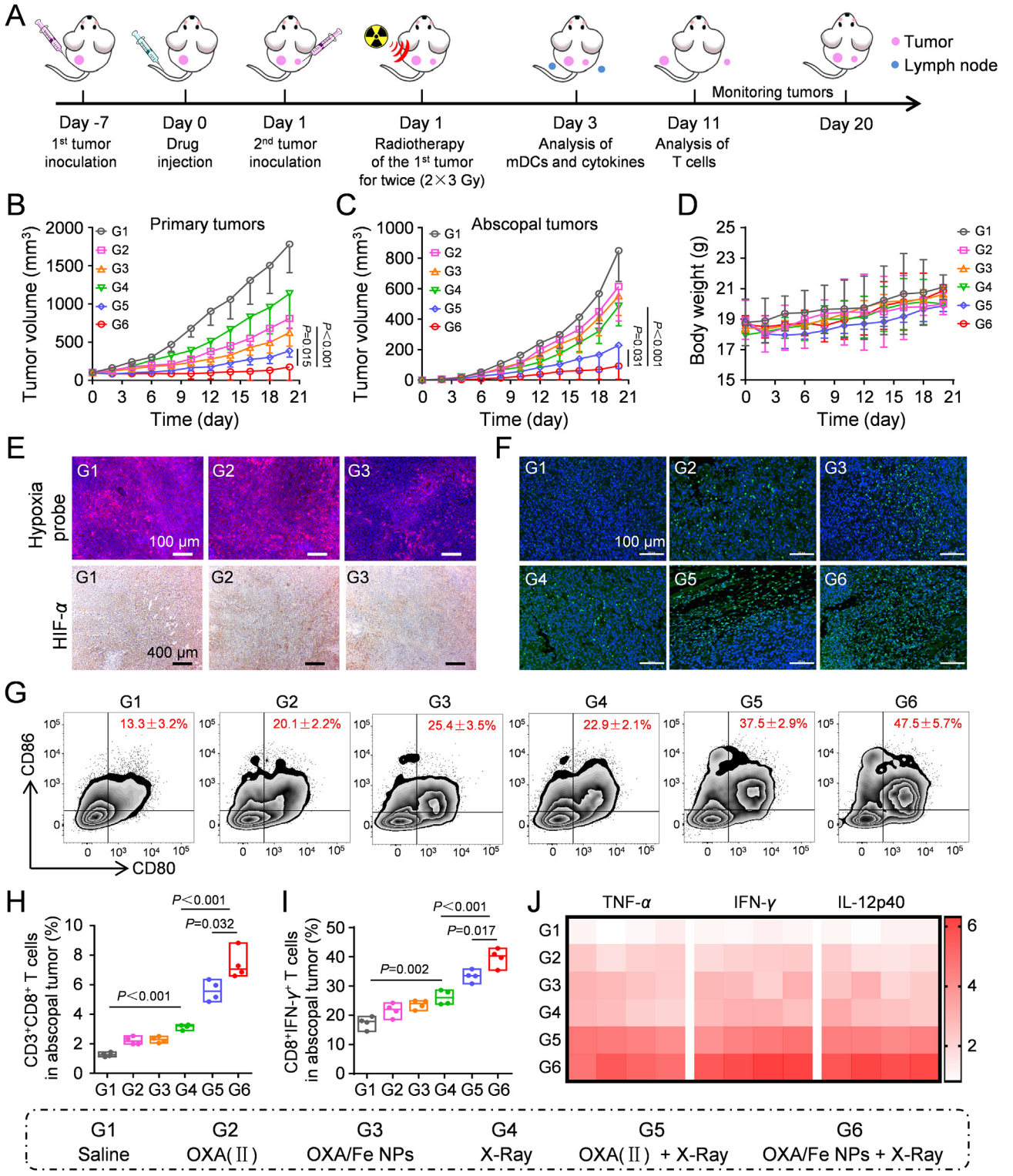

Figure 4 *In vivo* therapeutic efficacy of bimetallic NPs-amplified radio-immunotherapy on combined bilateral tumor model. (A) Schematic illustration of experiment design; (B, C) Tumor growth curves of the primary and abscopal tumors in BALB/c mice; (D) Body weight change of CT26 tumor-bearing mice following the indicated treatments during the study; (E) Immunofluorescence of hypoxic (red) staining images of tumors and immunohistochemical of HIF-1α staining images of tumors from CT26 tumor-bearing mice at 48 h after intravenous injection of different formulations; (F) Immunofluorescence of CRT staining images of tumors from CT26 tumor-bearing mice; (G) The $CD80^+CD86^+$ DCs on $CD45^+CD11c^+$ cells gate within TDLNs on Day 3 by Flow cytometry; The percentages of (H) $CD8^+$ T cells and (I) $CD8^+$ T IFN-γ^+ cells populations within abscopal tumor tissues; (J) Cytokine levels of TNF-α, IFN-γ, and IL-12p40 in sera from mice isolated on Day 3 post various treatments. Data are presented as mean values ± SD (n = 4).

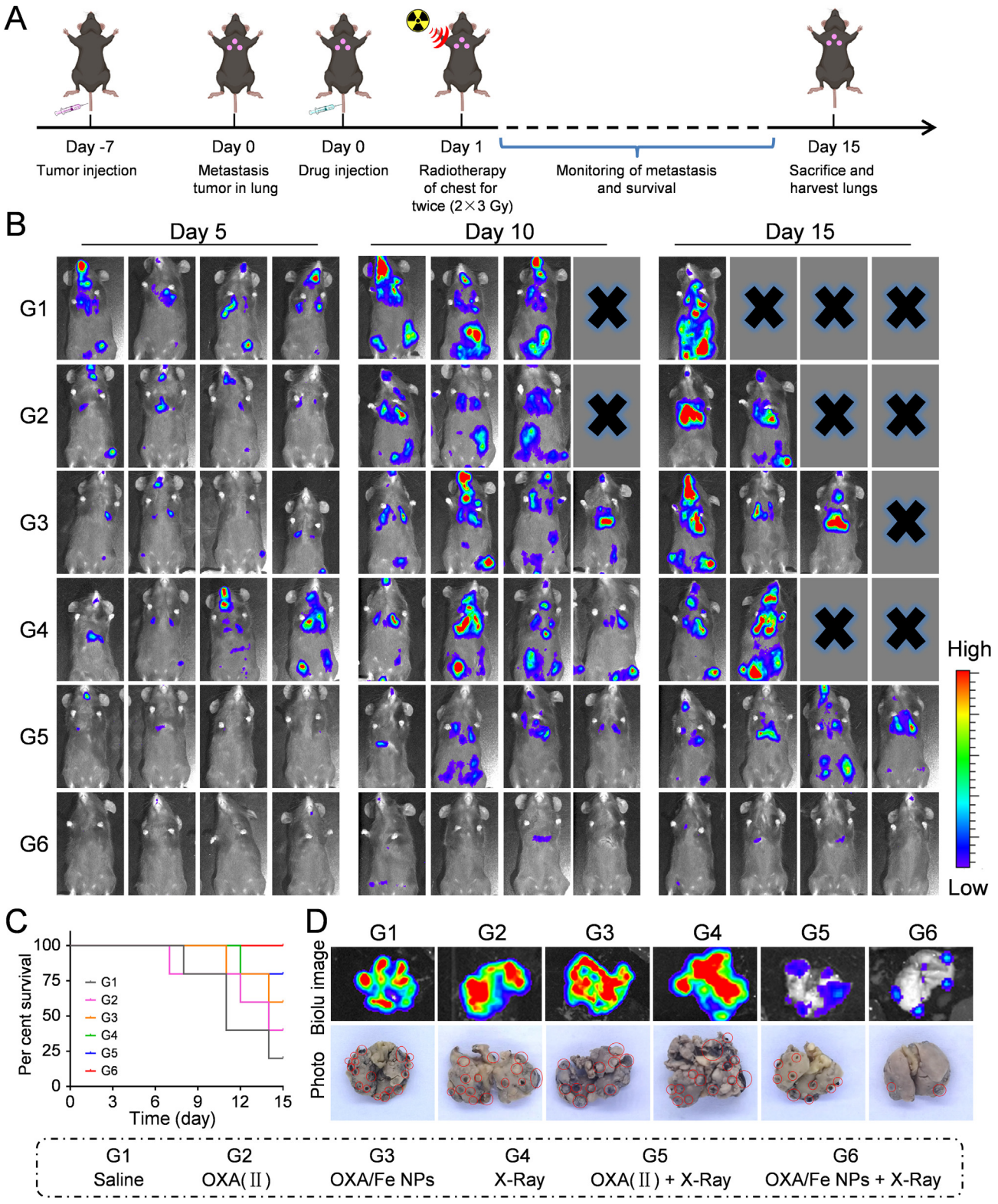

Figure 5 *In vivo* therapeutic efficacy of bimetallic NPs-amplified radio-immunotherapy on lung metastasis model. (A) Schematic illustration of OXA/Fe NPs-amplified radio-immunotherapy to inhibit spontaneous tumor metastases on the B16 breast tumor model. (B) *In vivo* bioluminescence images (on Days 5, 10, and 15) to track cancer metastases in different groups of mice after various treatments. (C) Survival of mice bearing B16 tumors with spontaneous metastases after various treatments ($n = 5$ per group). (D) Representative lung metastatic nodule specimens from mice.

3.7. *Bimetallic NPs activate long-term antitumor immune memory after low-dose RT*

Immunological memory, a hallmark of the adaptive immune response, provides long-term protection against previously encountered pathogens, including tumor cells[54,55]. The strength of immunological memory is intricately tied to the activation of DCs. Upon uptake and processing of antigens, DCs facilitate the activation of naive T cells (Th0), leading to their subsequent proliferation and differentiation into effector T cells and memory T cells[56]. In the subcutaneous combined bilateral tumor model and lung metastasis tumor model, the oxaliplatin-based chemotherapy (OXA and OXA/Fe NPs) combined with low-dose RT was demonstrated to suppress tumors and activate immune response more effectively than chemotherapy and RT alone. Hence, a 4T1 recurrent tumor model was further utilized to assess the potential induction of immunological memory by OXA/Fe NPs-amplified radio-immunotherapy (Fig. 6A). On Day 15 after different treatments, the mice were re-challenged with the second batch of 4T1 cells (2×10^5 cells per mouse). In the surgery group, the growth of the re-challenged tumor appeared to be rather fast. In contrast, the growth of re-challenged tumors in mice treated with OXA/Fe NPs-amplified radio-immunotherapy was remarkably inhibited (Fig. 6B, Supporting Information Figs. S39 and S40).

Next, a series of analyses were carried out to investigate the robust anti-tumor immune memory generated after OXA/Fe NPs plus X-ray irradiation. The memory T cells in the spleen were harvested and analyzed on Day 15 before being re-challenged with secondary tumors (Supporting Information Fig. S41). Effector memory T cells (T_{EM} cells), which reside in both lymphoid and nonlymphoid tissues, can induce a strong immune memory protection effect by producing multiple cytokines like TNF-α and IFN-γ upon a second encounter with the same antigen[57,58]. The percentages of T_{EM} cells ($CD3^+CD8^+CD62L^-CD44^+$) in the OXA/Fe NPs plus X-ray irradiation group were ~70.3%, almost 2.97 folds compared to the surgery group (~23.1%) and 1.33 folds compared to the OXA (II) plus X-ray irradiation group (~53.0%) (Fig. 6C). The cytokines in the sera of mice with different treatments were also analyzed by ELISA. The serum levels of IL-12p40, IFN-γ, and TNF-α were significantly increased in the mice treated with OXA/Fe NPs

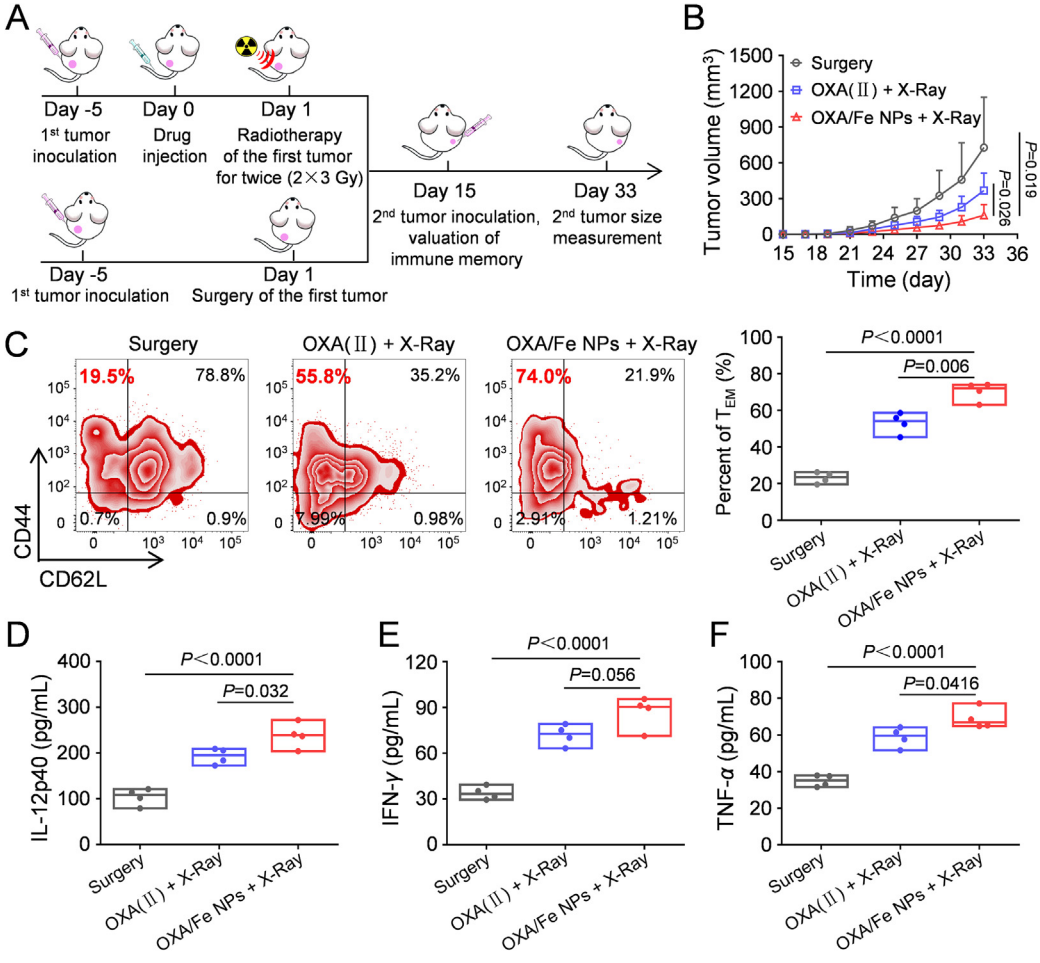

Figure 6 Bimetallic NPs activate long-term antitumor immune memory after low-dose RT. (A) Schematic illustration of experiment design to investigate the long-term immune-memory effect by OXA/Fe NPs-amplified radio-immunotherapy; (B) Tumor growth curves of re-challenged tumors inoculated 14 days post-eliminated of their first tumors by surgery or OXA/Fe NPs plus X-ray irradiation (Day 15); (C) Proportions of effector memory T cells (T_{EM}) in the spleen analyzed by flow cytometry (gated on $CD3^+CD8^+CD62L^-CD44^+$ T cells) on Day 15 before re-challenging mice with secondary tumors; Cytokine levels of (D) IL-12p40 (E) TNF-α, and (F) IFN-γ in sera from mice isolated on Day 15 before re-challenging mice with secondary tumors. Data are presented as mean values ± SD ($n = 4$).

plus X-ray irradiation (Fig. 6D and F), indicating the successful establishment of antitumor immune memory responses in this group. Thus, all the above results revealed that OXA/Fe NPs-amplified radio-immunotherapy could activate immune cells and cytokines release to maintain and promote immune cell proliferation and induce an excellent long-term immune protective effect.

4. Conclusions

In conclusion, we have reported bimetallic nanoparticles (OXA/Fe NPs) as a cascade sensitizing amplifier for low-dose and robust cancer radio-immunotherapy. Our study demonstrates that the OXA/Fe NPs exhibit tumor-specific accumulation and activation of drugs in response to the reductive and acidic microenvironment within tumor cells. The released OXA (II) can sensitize cancer cells to RT by inducing DNA damage. Simultaneously, both OXA (II) and RT contribute to an elevation in H_2O_2 level, which facilitates the Fe-initiated Fenton-type Haber−Weiss reaction to increase ROS and O_2 levels, further amplifying the sensitization effect of RT. The cascade reaction can synergistically amplify the ICD effect of tumor cells, thereby promoting DC maturation and leading to a potent antitumor immune response. The OXA/Fe NPs-based low-dose (6 Gy) radio-immunotherapy achieved a remarkable synergistic therapeutic effect to inhibit distant and metastatic tumors, and provided long-term immune memory protection against tumor recurrence in a recurrent 4T1 tumor model. Our findings propose a promising strategy to enhance antitumor immunity of low-dose radiotherapy by amplifying tumor radio-sensitivity and immunogenicity, offering great potential in clinical application and translational prospects.

Acknowledgments

This work is supported by grants from the National Natural Science Foundation of China (Nos. 22275081, and 82372117), Guangdong Basic and Applied Basic Research Foundation (2021B1515120065, China), Guangzhou Science and Technology Bureau (202206010068), the Natural Science Foundation of Hebei Province (E2023205004, China), and China Postdoctoral Science Foundation (2022M711532 and 2022T150302).

Author contributions

Dongfang Zhou and Yupeng Wang designed the project. Yupeng Wang, Lina Wang, Tao Li, Min Ouyang and Hejian Xiong performed the experiments. Dongfang Zhou, Yupeng Wang and Hejian Xiong analyzed and interpreted the data. Dongfang Zhou supervised the overall research. Dongfang Zhou, Yupeng Wang and Hejian Xiong wrote the manuscript with input from all coauthors.

Conflicts of interest

The authors declare no competing financial interest.

Appendix A. Supporting information

Supporting data to this article can be found online at https://doi.org/10.1016/j.apsb.2023.11.028.

References

1. Atun R, Jaffray DA, Barton MB, Bray F, Baumann M, Vikram B, et al. Expanding global access to radiotherapy. *Lancet Oncol* 2015;**16**:1153−86.
2. Baumann M, Krause M, Overgaard J, Debus J, Bentzen SM, Daartz J, et al. Radiation oncology in the era of precision medicine. *Nat Rev Cancer* 2016;**16**:234−49.
3. Babaei M, Ganjalikhani M. The potential effectiveness of nanoparticles as radio sensitizers for radiotherapy. *Bioimpacts* 2014;**4**:15−20.
4. Herrera FG, Bourhis J, Coukos G. Radiotherapy combination opportunities leveraging immunity for the next oncology practice. *CA A Cancer J Clin* 2017;**67**:65−85.
5. Zhen WY, Weichselbaum RR, Lin WB. Nanoparticle-mediated radiotherapy remodels the tumor microenvironment to enhance antitumor efficacy. *Adv Mater* 2023;**35**:2206370.
6. Yang Y, Liu B, Liu Y, Chen JQ, Sun YJ, Pan XS, et al. DNA-based MXFs to enhance radiotherapy and stimulate robust antitumor immune responses. *Nano Lett* 2022;**22**:2826−34.
7. Li QQ, Shi ZQ, Zhang F, Zeng WW, Zhu DW, Mei L. Symphony of nanomaterials and immunotherapy based on the cancer-immunity cycle. *Acta Pharm Sin B* 2022;**12**:107−34.
8. Barker HE, Paget JTE, Khan AA, Harrington KJ. The tumour microenvironment after radiotherapy: mechanisms of resistance and recurrence. *Nat Rev Cancer* 2015;**15**:409−25.
9. Sang W, Xie LS, Wang GH, Li J, Zhang Z, Li B, et al. Oxygen-enriched metal-phenolic X-ray nanoprocessor for cancer radio-radiodynamic therapy in combination with checkpoint blockade immunotherapy. *Adv Sci* 2020;**8**:2003338.
10. Blair TC, Bambina S, Alice AF, Kramer GF, Medler TR, Baird JR, et al. Dendritic cell maturation defines immunological responsiveness of tumors to radiation therapy. *J Immunol* 2020;**204**:3416−24.
11. Vitale I, Shema E, Loi S, Galluzzi L. Intratumoral heterogeneity in cancer progression and response to immunotherapy. *Nat Med* 2021;**27**:212−24.
12. Xu YY, Xiong JY, Sun XY, Gao HL. Targeted nanomedicines remodeling immunosuppressive tumor microenvironment for enhanced cancer immunotherapy. *Acta Pharm Sin B* 2022;**12**:4327−47.
13. Huang ZS, Wang YX, Yao D, Wu JH, Hu YQ, Yuan A. Nanoscale coordination polymers induce immunogenic cell death by amplifying radiation therapy mediated oxidative stress. *Nat Commun* 2021;**12**:145.
14. Sang W, Zhang Z, Wang GH, Xie LS, Li J, Li WX, et al. A triple-kill strategy for tumor eradication reinforced by metal-phenolic network nanopumps. *Adv Funct Mater* 2022;**32**:2113168.
15. Zhang PS, Meng JL, Li YY, Yang C, Hou Y, Tang W, et al. Nanotechnology-enhanced immunotherapy for metastatic cancer. *Innovation* 2021;**2**:100147.
16. De Ruysscher D, Niedermann G, Burnet NG, Siva S, Lee AWM, Hegi-Johnson F. Radiotherapy toxicity. *Nat Rev Dis Prim* 2019;**5**:13.
17. Uribe-Herranz M, Rafail S, Beghi S, Gil-de-Gomez L, Verginadis I, Bittinger K, et al. Gut microbiota modulate dendritic cell antigen presentation and radiotherapy-induced antitumor immune response. *J Clin Invest* 2020;**130**:466−79.
18. Hwang WL, Pike LR, Royce TJ, Mahal BA, Loeffler JS. Safety of combining radiotherapy with immune-checkpoint inhibition. *Nat Rev Clin Oncol* 2018;**15**:477−94.
19. Gillison ML, Trotti AM, Harris J, Eisbruch A, Harari PM, Adelstein DJ, et al. Radiotherapy plus cetuximab or cisplatin in human papillomavirus-positive oropharyngeal cancer (NRG Oncology RTOG 1016): a randomised, multicentre, non-inferiority trial. *Lancet* 2020;**395**:784.
20. Li WX, Yan J, Tian H, Li B, Wang GH, Sang W, et al. A platinum@polymer-catechol nanobraker enables radio-immunotherapy for crippling melanoma tumorigenesis, angiogenesis, and radioresistance. *Bioact Mater* 2023;**22**:34−46.
21. Xiao XH, Wang YP, Chen JY, Qin P, Chen PY, Zhou DF, et al. Self-targeting platinum(IV) amphiphilic prodrug nano-assembly as

radiosensitizer for synergistic and safe chemoradiotherapy of hepatocellular carcinoma. *Biomaterials* 2022;**289**:121793.
22. Sun LL, Shen FY, Tian LL, Tao HQ, Xiong ZJ, Xu J, et al. ATP-responsive smart hydrogel releasing immune adjuvant synchronized with repeated chemotherapy or radiotherapy to boost antitumor immunity. *Adv Mater* 2021;**33**:2007910.
23. Liu XQ, Liang S, Sang X, Chang LL, Fu SL, Yang H, et al. On-demand integrated nano-engager converting cold tumors to hot *via* increased DNA damage and dual immune checkpoint inhibition. *Acta Pharm Sin B* 2023;**13**:1740−54.
24. Zhang LP, Montesdeoca N, Karges J, Xiao HH. Immunogenic cell death inducing metal complexes for cancer therapy. *Angew Chem Int Ed* 2023;**62**:e202300662.
25. Wang WW, Wu L, Zhang JS, Wu HG, Han EK, Guo Q. Chemo-immunotherapy by combining oxaliplatin with immune checkpoint blockades reduced tumor burden in colorectal cancer animal model. *Biochem Bioph Res Co* 2017;**487**:1−7.
26. Guo JF, Yu Z, Das M, Huang L. Nano codelivery of oxaliplatin and folinic acid achieves synergistic chemo-immunotherapy with 5-fluorouracil for colorectal cancer and liver metastasis. *ACS Nano* 2020;**14**:5075−89.
27. Li SS, Shang L, Xu BL, Wang SH, Gu K, Wu QY, et al. A nanozyme with photo-enhanced dual enzyme-like activities for deep pancreatic cancer therapy. *Angew Chem Int Ed* 2019;**131**:12754−61.
28. Liu, Peng Y, Ding JS, Zhou WH. Fenton metal nanomedicines for imaging-guided combinatorial chemodynamic therapy against cancer. *Asian J Pharm Sci* 2022;**17**:177−92.
29. Hauser AK, Mitov MI, Daley EF, McGarry RC, Anderson KW, Hilt JZ. Targeted iron oxide nanoparticles for the enhancement of radiation therapy. *Biomaterials* 2016;**105**:127−35.
30. Chen K, Zhou RY, Liang HJ, Liao Y, Zhu S, Dong XH, et al. Reversing the pathological microenvironment by radiocatalytic sensitizer for local orthotopic osteosarcoma radiotherapy enhancement. *Nano Today* 2023;**48**:101739.
31. Wang WJ, Ling YY, Zhong YM, Li ZY, Tan CP, Mao ZW. Ferroptosis-enhanced cancer immunity by a ferrocene-appended iridium (III) diphosphine complex. *Angew Chem Int Ed* 2022;**61**:e202115247.
32. Yang YX, Zuo SY, Li LX, Kuang X, Li JB, Sun BJ, et al. Iron-doxorubicin prodrug loaded liposome nanogenerator programs multimodal ferroptosis for efficient cancer therapy. *Asian J Pharm Sci* 2021;**16**:784−93.
33. Fu LH, Wan YL, Qi C, He J, Li CY, Yang C, et al. Nanocatalytic theranostics with glutathione depletion and enhanced reactive oxygen species generation for efficient cancer therapy. *Adv Mater* 2021;**33**:2006892.
34. Gao YA, Zhao QY, Dong HL, Xiao M, Huang XF, Wu XJ. Developing acid-responsive glyco-nanoplatform based vaccines for enhanced cytotoxic T-lymphocyte responses against cancer and SARS-CoV-2. *Adv Funct Mater* 2021;**31**:2105059.
35. Sun J, Liang XL, Cai MY, Yan LB, Chen ZJ, Guo L, et al. Protein-crowned micelles for targeted and synergistic tumor-associated macrophage reprogramming to enhance cancer treatment. *Nano Lett* 2022;**22**:4410−20.
36. Yang LX, Xiao HH, Yan LS, Wang R, Huang YB, Xie ZG, et al. Lactose targeting oxaliplatin prodrug loaded micelles for more effective chemotherapy of hepatocellular carcinoma. *J Mater Chem B* 2014;**2**:2097−106.
37. Yamashita T, Hayes P. Analysis of XPS spectra of Fe^{2+} and Fe^{3+} ions in oxide materials. *Appl Surf Sci* 2008;**254**:2441.
38. Peng SJ, Xiao FF, Chen MW, Gao HL. Tumor-microenvironment-responsive nanomedicine for enhanced cancer immunotherapy. *Adv Sci* 2021;**9**:2103836.
39. Shen FY, Tao DL, Peng R, He Y, Liu Z, Ji JS, et al. Immunogenic nanomedicine based on GSH-responsive nanoscale covalent organic polymers for chemo-sonodynamic therapy. *Biomaterials* 2022;**283**:121428.
40. Gang X, Zhu H, Shi Y, Tang W. *In vitro* binding of an orally active platinum antitumor drug, JM216 to metallothionein. *Biometals* 2001;**14**:51−7.
41. Cong YW, Xiao HH, Xiong HJ, Wang ZG, Ding JX, Li C, et al. Dual drug backboned shattering polymeric theranostic nanomedicine for synergistic eradication of patient-derived lung cancer. *Adv Mater* 2018;**30**:1706220.
42. Dai YL, Yang Z, Cheng SY, Wang ZL, Zhang RL, Zhu GZ, et al. Toxic reactive oxygen species enhanced synergistic combination therapy by self-assembled metal-phenolic network nanoparticles. *Adv Mater* 2018;**30**:1704877.
43. Wang YP, Cong YW, Cai MY, Liang XL, Wang LN, Zhou DF. Charge-conversional click polyprodrug nanomedicine for targeted and synergistic cancer therapy. *J Control Release* 2023;**356**:567−79.
44. Liu JN, Bu WB, Shi JL. Chemical design and synthesis of functionalized probes for imaging and treating tumor hypoxia. *Chem Rev* 2017;**117**:6160−224.
45. Luan SY, Xie R, Yang YS, Xiao X, Zhou JF, Li XK, et al. Acid-responsive aggregated gold nanoparticles for radiosensitization and synergistic chemoradiotherapy in the treatment of esophageal cancer. *Small* 2022;**18**:2200115.
46. Vaes RDW, Hendriks LEL, Vooijs M, De Ruysscher D. Biomarkers of radiotherapy-induced immunogenic cell death. *Cells* 2021;**10**:930.
47. Gasteiger G, Ataide M, Kastenmüller W. Lymph node—an organ for T-cell activation and pathogen defense. *Immunol Rev* 2016;**271**:200−20.
48. Zhang JL, Sun XY, Zhao XF, Yang CR, Shi MH, Zhang BZ, et al. Combining immune checkpoint blockade with ATP-based immunogenic cell death amplifier for cancer chemo-immunotherapy. *Acta Pharm Sin B* 2022;**12**:3694−709.
49. Li Z, Li WP, Jiang SP, Hu C, Huang YY, Shevtsov M, et al. Legumain-triggered aggregable gold nanoparticles for enhanced intratumoral retention. *Chin Chem Lett* 2023;**34**:107518.
50. Stenger S, Hanson DA, Teitelbaum R, Dewan P, Niazi KR, Froelich CJ, et al. An antimicrobial activity of cytolytic T cells mediated by granulysin. *Science* 1998;**282**:121−5.
51. Bedoui S, Heath WR, Mueller SN. $CD4^+$ T-cell help amplifies innate signals for primary $CD8^+$ T-cell immunity. *Immunol Rev* 2016;**272**:52−64.
52. Kruse B, Buzzai AC, Shridhar N, Braun AD, Gellert S, Knauth K, et al. $CD4^+$ T cell-induced inflammatory cell death controls immune-evasive tumours. *Nature* 2023;**618**:1033−40.
53. Xu J, Xu LG, Wang CY, Yang R, Zhuang Q, Han X, et al. Near-Infrared-triggered photodynamic therapy with multitasking upconversion nanoparticles in combination with checkpoint blockade for immunotherapy of colorectal cancer. *ACS Nano* 2017;**11**:4463−74.
54. Teixeiro E, Daniels MA, Hamilton SE, Schrum AG, Bragado R, Jameson SC, et al. Different T cell receptor signals determine $CD8^+$ memory *versus* effector development. *Science* 2009;**323**:502−5.
55. Huang QZ, Wu X, Wang ZM, Chen XY, Wang LS, Lu YJ, et al. The primordial differentiation of tumor-specific memory $CD8^+$ T cells as bona fide responders to PD-1/PD-L1 blockade in draining lymph nodes. *Cell* 2022;**185**:4049.
56. Wang YY, Xiang Y, Xin WX, Wang XW, Peng XC, Liu XQ, et al. Dendritic cell biology and its role in tumor immunotherapy. *J Hematol Oncol* 2020;**13**:107.
57. Kaech SM, Wherry EJ, Ahmed R. Effector and memory T-cell differentiation: implications for vaccine development. *Nat Rev Immunol* 2002;**2**:251−62.
58. Youngblood B, Hale JS, Kissick HT, Ahn E, Xu X, Wieland A, et al. Effector CD8 T cells dedifferentiate into long-lived memory cells. *Nature* 2017;**552**:404.